Electronic Supplementary Material (ESI) for Journal of Materials Chemistry C.

Electronic supplementary information

for

Electrically responsive structural transformations triggered by vapour and temperature in a series of pleochroic bis(oxalato)chromium(III) complex salts

Marko Dunatov,[a] Andreas Puškarić,[a] Luka Pavić,[a] Zoran Štefanić[a] and Lidija Androš Dubraja*[a]

[1]Ruđer Bošković Institute, Bijenička cesta 54, 10000 Zagreb, Croatia

Contents

Table S1. Crystallographic data and structure refinement details for compound **1**$_{H_2O}$, **2**$_{H_2O}$, **3**$_{MeOH}$, **3**, **4**$_{H_2O}$, **4**, **5**$_{H_2O}$, and **6**$_{H_2O}$ 3

Table S2. Crystallographic data and structure refinement details for compound **1** and **3**$_{H_2O}$ 4

Figure S1. Room temperature XRPD pattern and profile fitting results for **1** 5

Figure S2. Room temperature XRPD pattern and profile fitting results for **3**$_{H_2O}$ 5

Figure S3. XRPD patterns of **1**, **1**$_{H_2O}$ and corresponding calculated patterns from single-crystal X-ray diffraction data 6

Figure S4. XRPD patterns of **2** and **2**$_{H_2O}$ 6

Figure S5. XRPD patterns of **3**, **3**$_{H_2O}$, **3**$_{MeOH}$ and corresponding calculated patterns from single-crystal X-ray diffraction data 7

Figure S6. XRPD patterns of **4**$_{H_2O}$ at 293 and 363 K, and **4** at 378 and 383 K 7

Figure S7. Pleochroism in complex salts **1**$_{H_2O}$ (a), **3**$_{MeOH}$ (b), **5**$_{H_2O}$ (c) and **6**$_{H_2O}$ (d) 8

Figure S8. ATR spectra of **1** and **1**$_{H_2O}$ 9

Figure S9. ATR spectra of **2** and **2**$_{H_2O}$ 9

Figure S10. ATR spectra of **3**, **3**$_{MeOH}$ and **3**$_{H_2O}$ 9

Figure S11. ATR spectrum of **4**$_{H_2O}$ 10

Figure S12. ATR spectrum of **5**$_{H_2O}$ 10

Figure S13. ATR spectrum of **6**$_{H_2O}$ 10

Figure S14. *In situ* ATR spectra following the drying and wetting proces of compound **1** at 298 K and atmosperic pressure 11

Figure S15. *In situ* ATR spectra following the drying and recovery (exposure to MeOH vapour) process of compound **3**$_{MeOH}$ at 25 °C and atmosperic pressure (a). *In situ* ATR spectra following the wetting and drying process of compound **3**$_{H2O}$ at at 298 K and atmosperic pressure (b) 11

Figure S16. TGA and DTA curves for compounds: **1** and **2** (a), **3**$_{H_2O}$ (b) and **4**$_{H_2O}$–**6**$_{H_2O}$ (c) measured under a synthetic air atmosphere 12

Figure S17. Temperature dependence of the dielectric loss during heating (dark red symbols) and cooling (blue symbols) cycles measured at 100 kHz frequency for compounds **1**, **3**$_{MeOH}$, **4**$_{H_2O}$, **5**$_{H_2O}$, and **6**$_{H_2O}$ 13

Figure S18. Temperature dependence of the dielectric constant during heating (dark red symbols) and cooling (blue symbols) cycles measured at 10 kHz frequency for compounds **3**$_{MeOH}$, **4**$_{H_2O}$, **5**$_{H_2O}$, and **6**$_{H_2O}$ 13

Figure S19. Temperature dependence of the dielectric loss during heating (dark red symbols) and cooling (blue symbols) cycles measured at 10 kHz frequency for compounds **3**$_{MeOH}$, **4**$_{H_2O}$, **5**$_{H_2O}$, and **6**$_{H_2O}$ 14

Figure S20. Frequency dependence of the dielectric constant for compounds **1**, **3**$_{MeOH}$, **4**$_{H_2O}$, **5**$_{H_2O}$, and **6**$_{H_2O}$ at 298 K 14

Table S1. Crystallographic data and structure refinement details for compound $\mathbf{1}_{H_2O}$, $\mathbf{2}_{H_2O}$, $\mathbf{3}_{MeOH}$, **3**, $\mathbf{4}_{H_2O}$, **4**, $\mathbf{5}_{H_2O}$, and $\mathbf{6}_{H_2O}$

Compound	$\mathbf{1}_{H_2O}$	$\mathbf{2}_{H_2O}$	$\mathbf{3}_{MeOH}$	**3**	$\mathbf{4}_{H_2O}$	**4**	$\mathbf{5}_{H_2O}$	$\mathbf{6}_{H_2O}$
Temperature/K	140	293	223	298	298	400	298	298
Crystal colour, habit	orange and purplish red, stick	orange and purplish red, prism	orange and purplish red, prism	red, prism	red, prism	red, prism	orange and purplish red, prism	orange and purplish red, prism
Empirical formula	$C_{34}H_{54}Cr_2N_6O_{28}$	$C_{38}H_{48}Cr_2N_6O_{25}$	$C_{22}H_{27}Cr_1N_4O_9$	$C_{21}H_{23}Cr_1N_4O_8$	$C_{21}H_{22}CrN_3O_{10}$	$C_{21}H_{20}CrN_3O_9$	$C_{22}H_{26}CrN_3O_{13}$	$C_{23}H_{26}CrN_3O_{12}$
M_r/g mol^{-1}	1098.80	1092.81	543.47	511.43	528.41	510.40	592.46	588.47
Crystal system	Triclinic	Triclinic	Monoclinic	Triclinic	Monoclinic	Monoclinic	Orthorombic	Monoclinic
Space group	$P\bar{1}$	$P\bar{1}$	$P2_1/c$	$P\bar{1}$	$P2_1/c$	$P2_1/c$	$Pbca$	$P2_1/c$
a/Å	12.2426(5)	10.4903(2)	15.8377(2)	9.5955(4)	15.4312(4)	15.875(2)	12.5654(1)	15.8032(1)
b/Å	13.2490(6)	13.9080(2)	14.9630(2)	9.7701(5)	11.8305(3)	10.325(2)	19.0980(1)	10.4129(1)
c/Å	15.9614(7)	17.7129(4)	9.9377(1)	12.4681(7)	13.3558(4)	14.072(2)	20.5684(1)	14.8291(1)
α/°	99.315(5)	97.152(2)	90	91.438(4)	90	90	90	90
β/°	100.091(5)	100.620(2)	93.667(1)	100.633(4)	110.515(3)	112.22(2)	90	93.612(1)
γ/°	107.873(4)	92.735(2)	90	107.230(4)	90	90	90	90
V/Å^3	2360.80(19)	2513.64(8)	2350.21(5)	1093.28(10)	2283.59(12)	2135.3(6)	4935.88(5)	2435.39(3)
Z	2	2	4	2	4	4	8	4
ρ_{calcd}/g cm^{-3}	1.546	1.432	1.536	1.554	1.537	1.588	1.595	1.605
μ/mm^{-1}	4.680	4.351	4.548	4.816	4.688	4.956	4.500	4.525
F(000)	1144	1096	1132	530	1092		2456	1220
θ range/°	3.60–80.61	3.21–76.47	5.35–77.16	3.62–74.86	3.05–75.87	5.23-78.66	4.73–75.88	5.09–75.84
Measured reflections	38971	26104	15683	7468	12391	9496	28808	13372
Independent reflections	10043	10392	4799	4281	4716	3778	5119	5020
Observed reflections	9364	9692	4570	3673	4160	2477	4872	4683
No. of parameters, restraints	710, 36	721, 2	355, 4	307, 0	332, 3	333, 6	364, 2	384, 8
R_{int}	0.0431	0.0272	0.0312	0.0597	0.0536	0.1069	0.0277	0.0338
R, wR [$I > 2\sigma(I)$]	0.0508, 0.1347	0.0577, 0.1737	0.0333, 0.0935	0.0573, 0.1616	0.0600, 0.1620	0.1564, 0.3248	0.0451, 0.1400	0.0406, 0.1026
R, wR [all data]	0.0537, 0.1366	0.0601, 0.1786	0.0347, 0.0946	0.0717, 0.1764	0.0650, 0.1729	0.2094, 0.3585	0.0465, 0.1419	0.0433, 0.1050
Goodness of fit	1.049	1.042	1.085	0.991	1.028	1.159	1.052	1.070
$\Delta\rho_{max}$, $\Delta\rho_{min}$/e Å^{-3}	0.676, -0.712	1.062; -0.410	0.295; -0.577	0.661; -0.636	0.763; -0.534	0.412; -0.769	0.544; -0.739	0.311; -0.570

Table S2. Crystallographic data and structure refinement details for compound **1** and $\mathbf{3}_{H_2O}$

Compound	**1**	$\mathbf{3}_{H_2O}$
Temperature/K	293	293
Crystal colour, habit	reddish, stick	reddish, prism
Empirical formula	$C_{34}H_{30}Cr_2N_6O_{16}$	$C_{21}H_{33}CrN_4O_{13}$
M_r/g mol^{-1}	882.64	601.50
Crystal system	Monoclinic	Monoclinic
Space group	$P2_1/c$	$P2_1/a$
a/Å	16.1963(12)	19.4728(7)
b/Å	16.75325(96)	12.6551(4)
c/Å	13.8097(10)	10.8221(4)
α/°	90	90
β/°	103.5740(46)	94.1606(3)
γ/°	90	90
V/Å^3	3642.45(44)	2659.89(17)
Z	4	4
ρ_{calcd}/g cm^{-3}	1.610	1.502
Step size/°	0.013	0.013
2θ range/°	5–70	6.4–50
R_p	0.0311	0.0401
R_{wp}	0.0402	0.048
R_{exp}	0.0230	0.016
Refined parameters	67	70
Background	Chebyshev polynomial of 6th order	

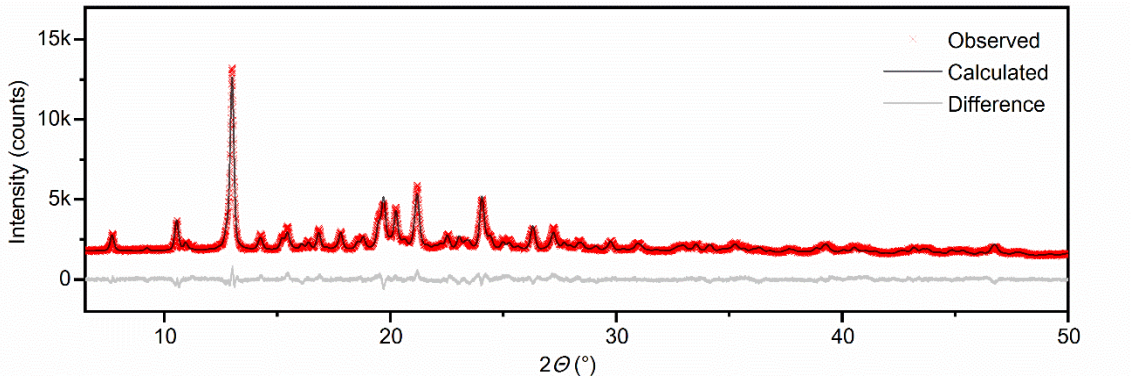

Figure S1. Room temperature XRPD pattern and profile fitting results for **1**

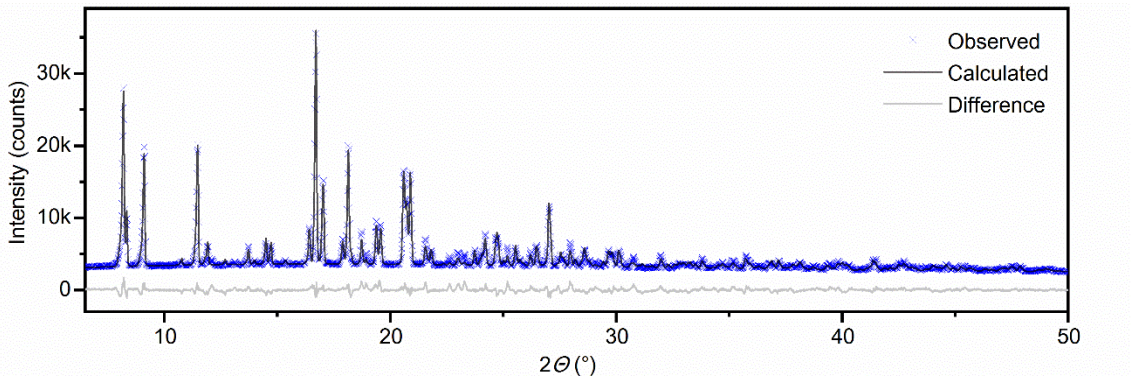

Figure S2. Room temperature XRPD pattern and profile fitting results for $\mathbf{3}_{H_2O}$

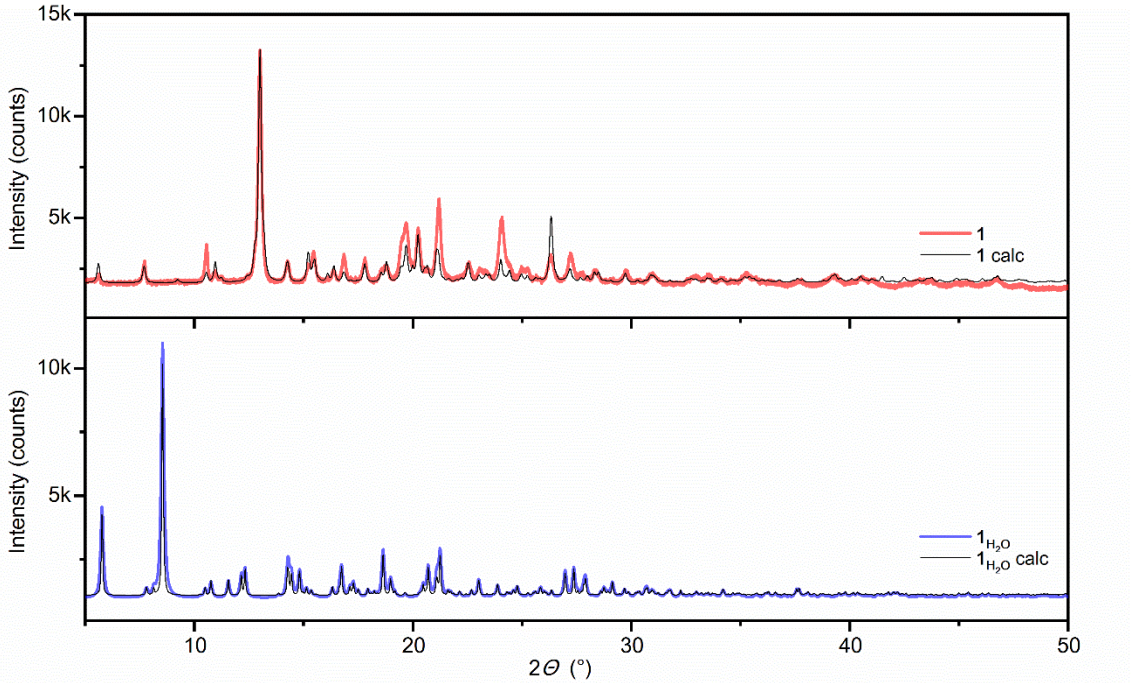

Figure S3. XRPD patterns of **1**, $\mathbf{1_{H2O}}$ and corresponding calculated patterns from single-crystal X-ray diffraction data

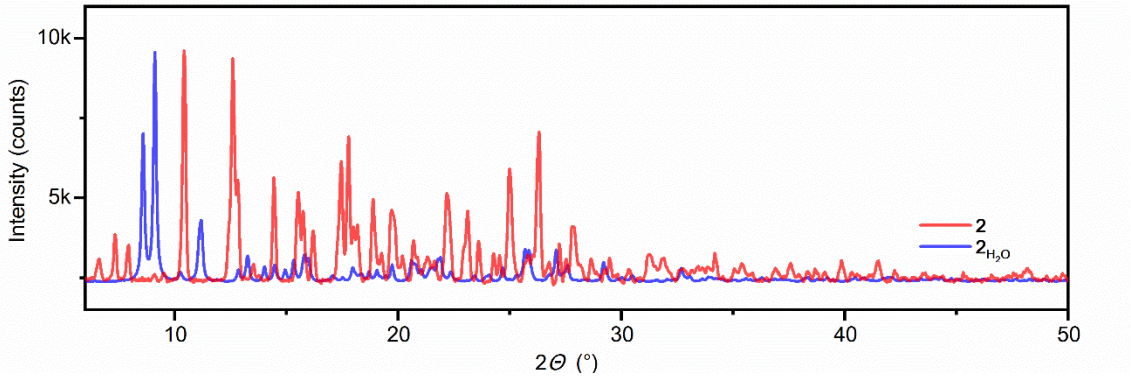

Figure S4. XRPD patterns of **2** and $\mathbf{2_{H2O}}$

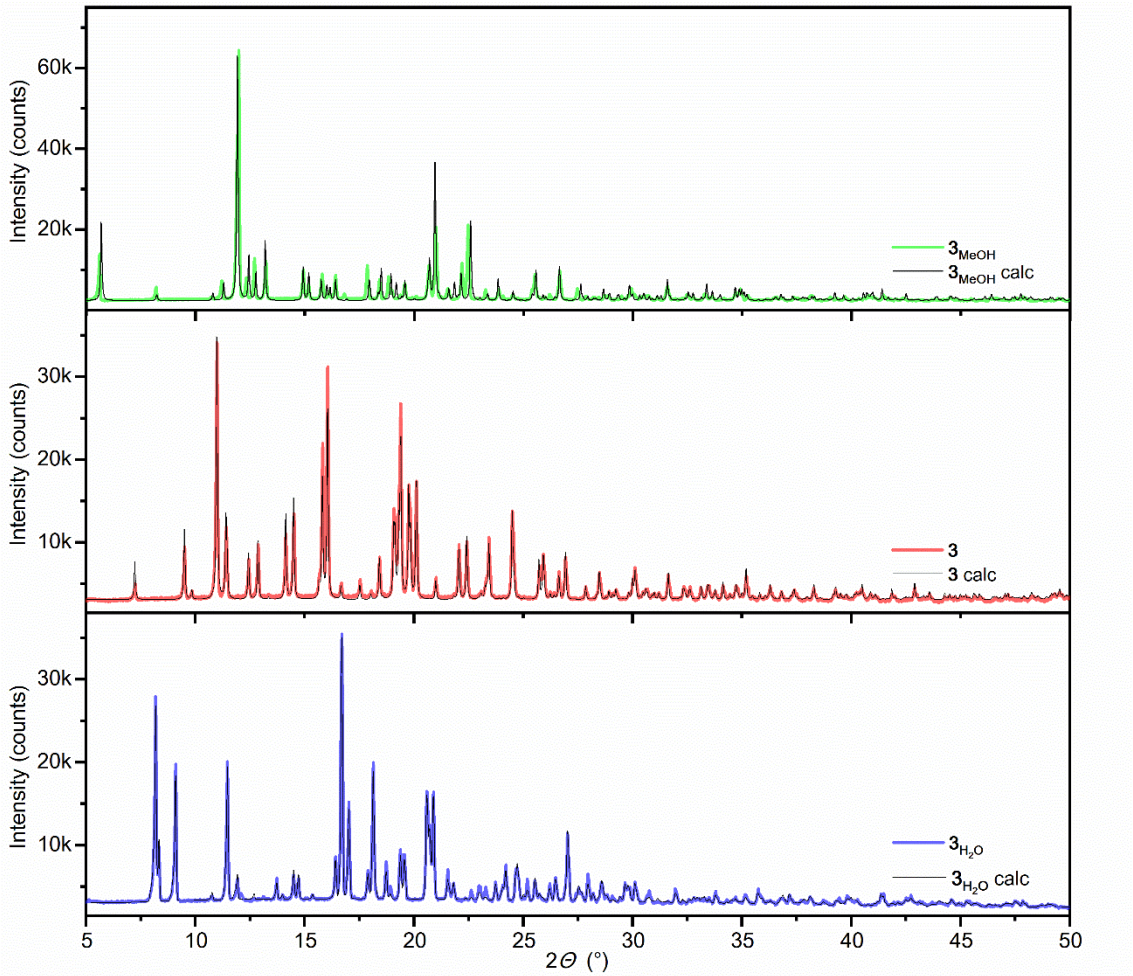

Figure S5. XRPD patterns of **3**, $\mathbf{3_{H2O}}$, $\mathbf{3_{MeOH}}$ and corresponding calculated patterns from single-crystal X-ray diffraction data

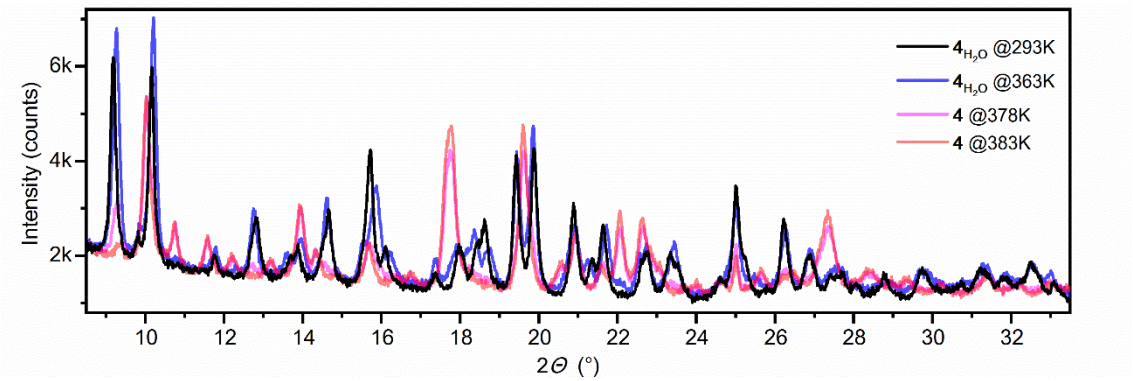

Figure S6. XRPD patterns of $\mathbf{4_{H2O}}$ at 293 and 363 K, and **4** at 378 and 383 K

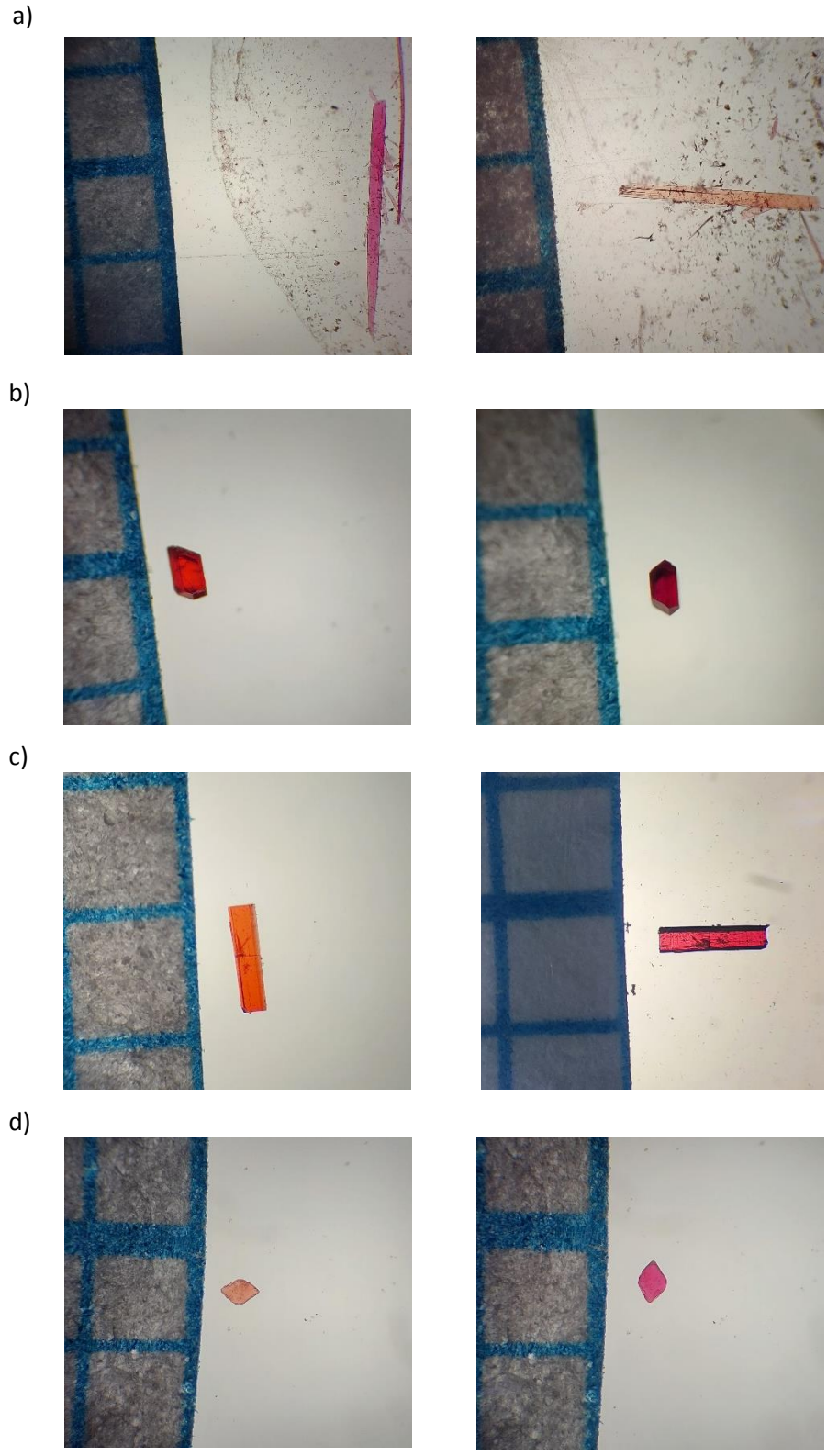

Figure S7. Pleochroism in complex salts $\mathbf{1}_{H2O}$ (a), $\mathbf{3}_{MeOH}$ (b), $\mathbf{5}_{H2O}$ (c) and $\mathbf{6}_{H2O}$ (d)

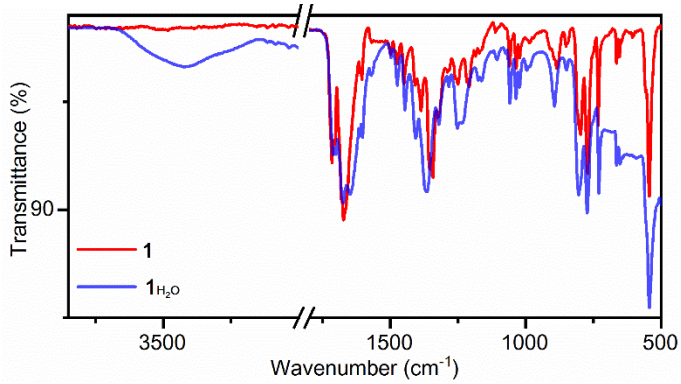

Figure S8. ATR spectra of **1** and $\mathbf{1_{H2O}}$

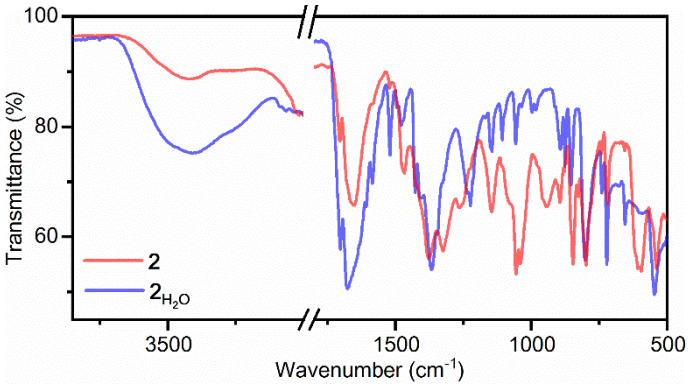

Figure S9. ATR spectra of **2** and $\mathbf{2_{H2O}}$

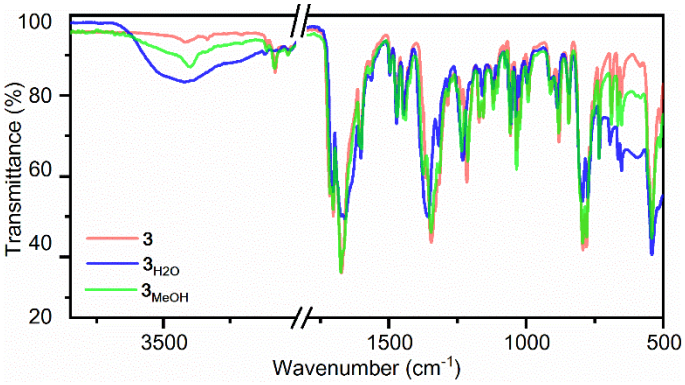

Figure S10. ATR spectra of **3**, $\mathbf{3_{MeOH}}$ and $\mathbf{3_{H2O}}$

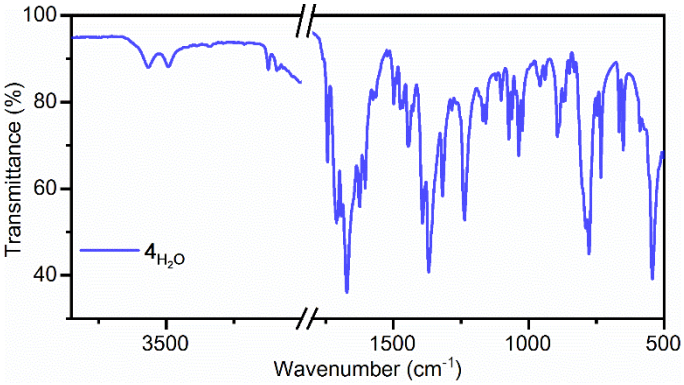

Figure S11. ATR spectrum of $\mathbf{4_{H2O}}$

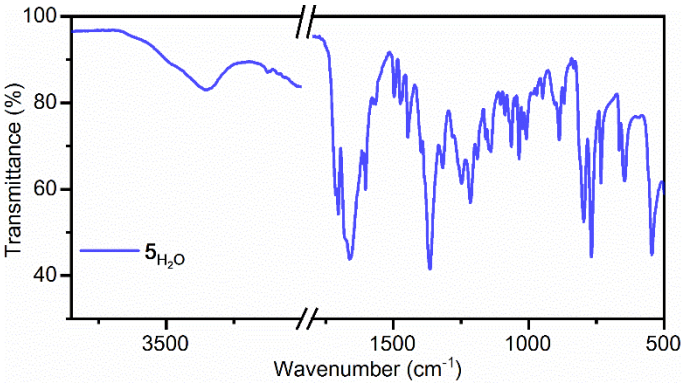

Figure S12. ATR spectrum of $\mathbf{5_{H2O}}$

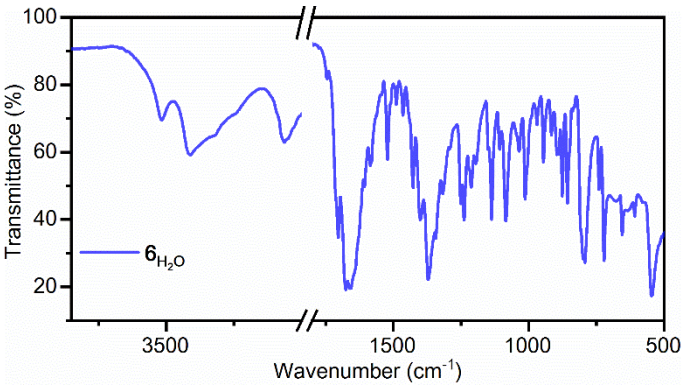

Figure S13. ATR spectrum of $\mathbf{6_{H2O}}$

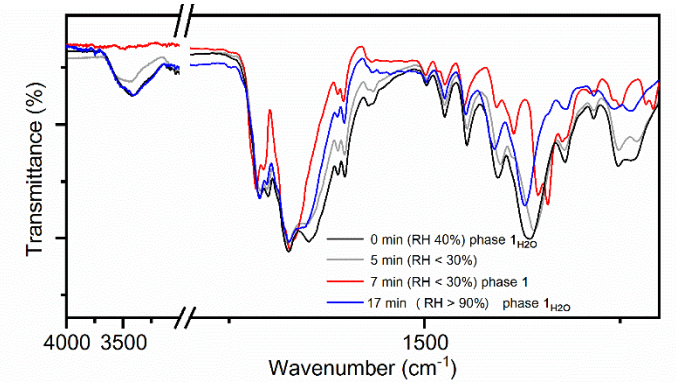

Figure S14. *In situ* ATR spectra following the drying and wetting proces of compound **1** at 298 K and atmosperic pressure

a)

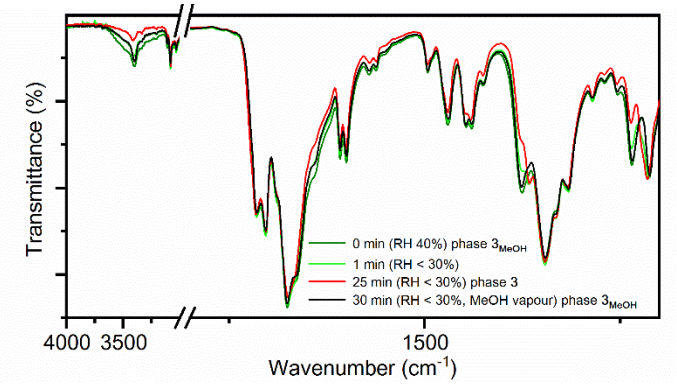

b)

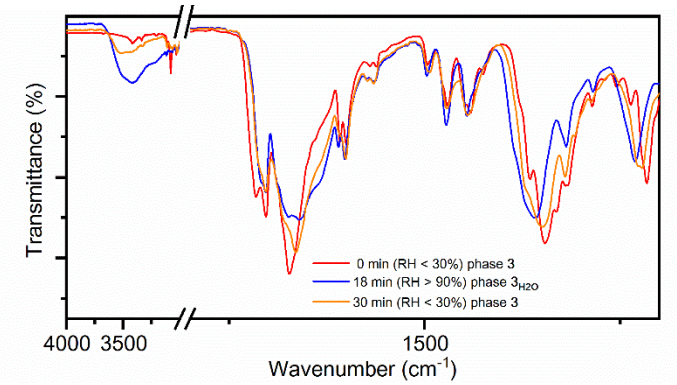

Figure S15. *In situ* ATR spectra following the drying and recovery (exposure to MeOH vapour) process of compound $\mathbf{3_{MeOH}}$ at 25 °C and atmosperic pressure (a). *In situ* ATR spectra following the wetting and drying process of compound $\mathbf{3_{H_2O}}$ at at 298 K and atmosperic pressure (b)

a)

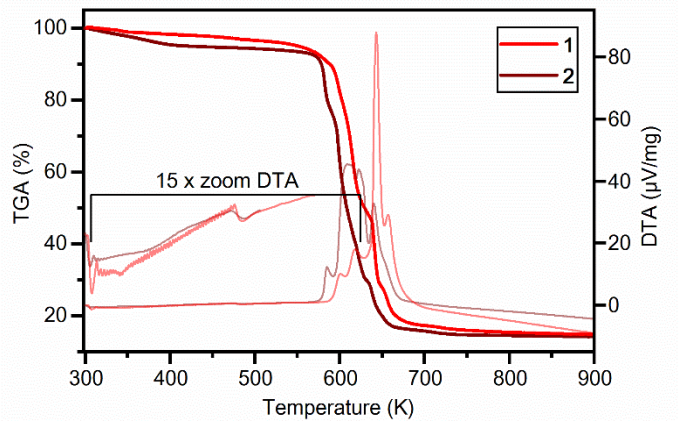

b)

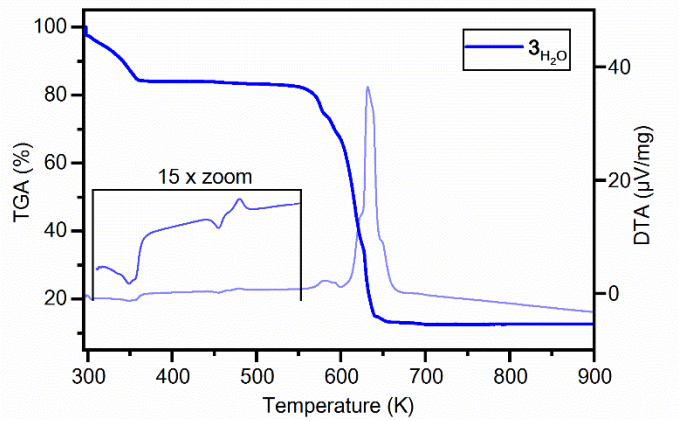

c)

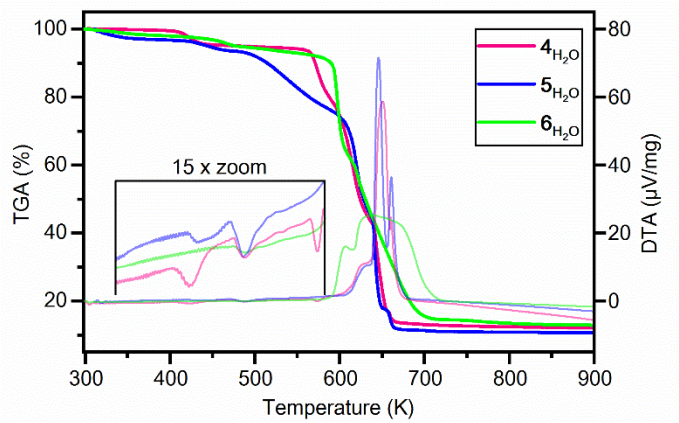

Figure S16. TGA and DTA curves for compounds: **1** and **2** (a), **3**$_{H_2O}$ (b) and **4**$_{H_2O}$–**6**$_{H_2O}$ (c) measured under a synthetic air atmosphere

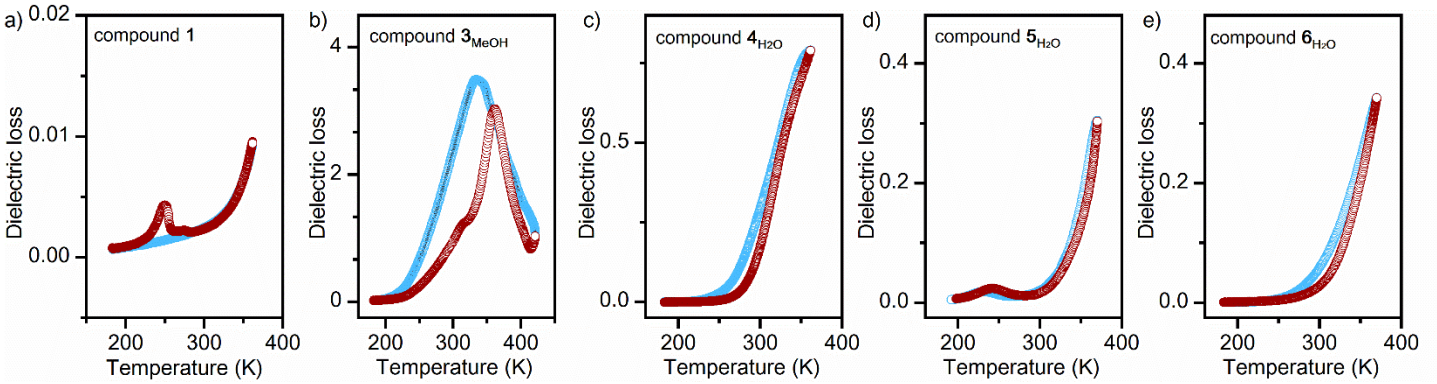

Figure S17. Temperature dependence of the dielectric loss during heating (dark red symbols) and cooling (blue symbols) cycles measured at 100 kHz frequency for compounds **1**, **3**$_{MeOH}$, **4**$_{H2O}$, **5**$_{H2O}$, and **6**$_{H2O}$

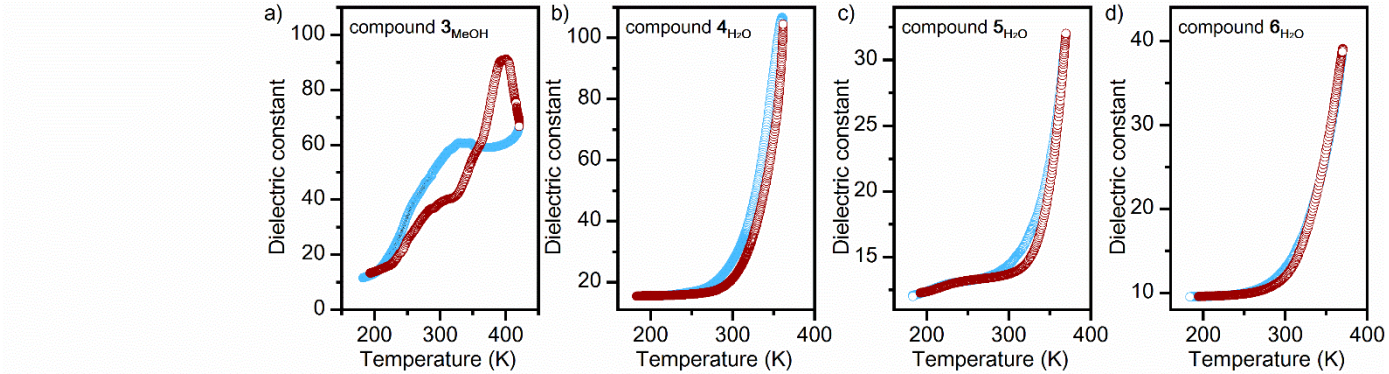

Figure S18. Temperature dependence of the dielectric constant during heating (dark red symbols) and cooling (blue symbols) cycles measured at 10 kHz frequency for compounds **3**$_{MeOH}$, **4**$_{H2O}$, **5**$_{H2O}$, and **6**$_{H2O}$

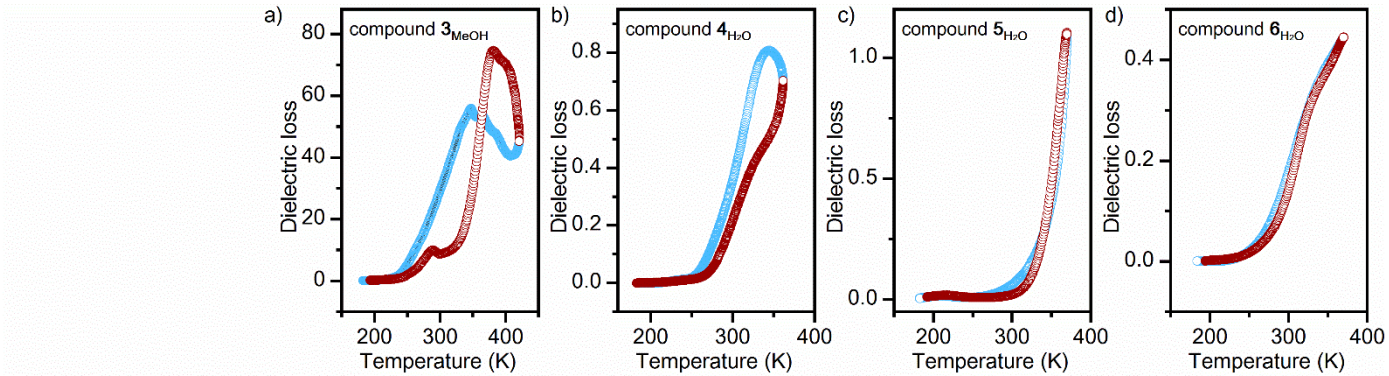

Figure S19. Temperature dependence of the dielectric loss during heating (dark red symbols) and cooling (blue symbols) cycles measured at 10 kHz frequency for compounds $\mathbf{3_{MeOH}}$, $\mathbf{4_{H2O}}$, $\mathbf{5_{H2O}}$, and $\mathbf{6_{H2O}}$

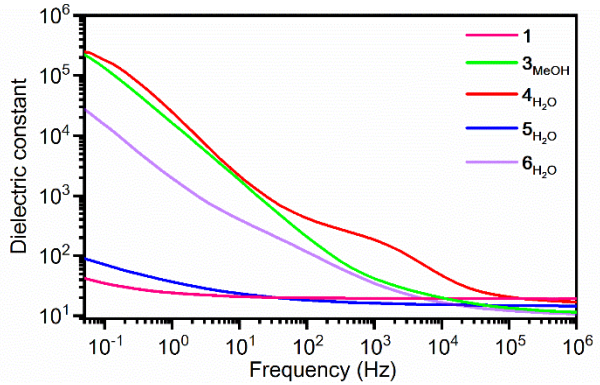

Figure S20. Frequency dependence of the dielectric constant for compounds **1**, $\mathbf{3_{MeOH}}$, $\mathbf{4_{H2O}}$, $\mathbf{5_{H2O}}$, and $\mathbf{6_{H2O}}$ at 298 K